

# A Multifunctional Contrast Agent for $^{19}\text{F}$ -Based Magnetic Resonance Imaging

Liang Du, Shannon Helsper, Neda Arabzadeh Nosratabad, Wentao Wang, Debra Ann Fadool, Catherine Amiens, Samuel Grant, and Hedi Mattoussi\*



Cite This: *Bioconjugate Chem.* 2022, 33, 881–891



Read Online

ACCESS |



Metrics & More

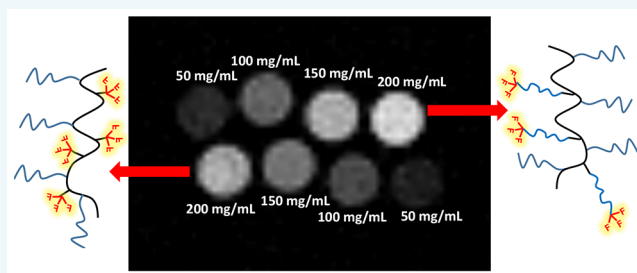


Article Recommendations



Supporting Information

**ABSTRACT:** Magnetic resonance imaging, MRI, relying on  $^{19}\text{F}$  nuclei has attracted much attention, because the isotopes exhibit a high gyromagnetic ratio (comparable to that of protons) and have 100% natural abundance. Furthermore, due to the very low traces of intrinsic fluorine in biological tissues, fluorine labeling allows easy visualization *in vivo* using  $^{19}\text{F}$ -based MRI. However, one of the drawbacks of the available fluorine tracers is their very limited solubility in water. Here, we detail the design and preparation of a set of water-compatible fluorine-rich polymers as contrast agents that can enhance the effectiveness of  $^{19}\text{F}$ -based MRI. The agents are synthesized using the nucleophilic addition reaction between poly(isobutylene-*alt*-maleic anhydride) copolymer and a mixture of amine-appended fluorine groups and polyethylene glycol (PEG) blocks. This allows control over the polymer architecture and stoichiometry, resulting in good affinity to water solutions. We further investigate the effects of introducing additional segmental mobility to the fluorine moieties in the polymer, by inserting a PEG linker between the moieties and the polymer backbone. We find that controlling the polymer stoichiometry and introducing additional segmental mobility enhance the NMR signals and narrow the peak profile. In particular, we assess the impact of the PEG linker on  $T_2^*$  and  $T_1$  relaxation times, using a series of gradient-recalled echo images with varying echo times, TE, or recovery time, TR, respectively. We find that for equivalent concentrations, the PEG linker greatly increases  $T_2^*$ , while maintaining high  $T_1$  values, as compared to polymers without this linker. Phantom images collected from these compounds show bright signals over a background with high intensities.



## INTRODUCTION

Magnetic resonance imaging (MRI) is a noninvasive technique with a wide range of applications in biology, medicine, and materials science.<sup>1–5</sup> For instance,  $^1\text{H}$ -based MRI enables the noninvasive visualization of soft and deep tissue, by exploiting the combination of high natural abundance and the large gyromagnetic ratio of protons, to allow the acquisition of images with good spatial resolution (submillimeter).<sup>2–4,6</sup> Indeed,  $^1\text{H}$ -based MRI has been used over the past three decades to acquire a large amount of data that consolidated its great clinical values in diagnostics and biomedicine.<sup>7,8</sup> It has also been shown that MRI provides highly informative data that can help in neuroscience and biomedicine, with particularly strong clinical applications in tumor diagnosis and localization.<sup>9,10</sup>  $^1\text{H}$ -based MRI relies on changes in the transverse ( $T_2$ ) and longitudinal ( $T_1$ ) spin relaxation properties of water protons distributed in living tissues. It is often employed in combination with a specially designed contrast agent (CA), which shortens the relaxation of proximal proton spins and enhances the image contrast and resolution. CAs such as those made from Gd(III) paramagnetic complexes and superparamagnetic iron oxide (SPIO) nanoparticles are widely used in proton-based MRI, but they still face practical

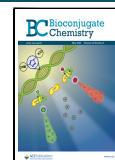
limitations. These CAs respectively affect the longitudinal ( $T_1$ ) or transverse ( $T_2$ ) relaxation times of the surrounding tissue, and their use requires pre- and postinjection imaging, resulting in long scan times, while yielding large background signals.<sup>11–14</sup> Moreover, relatively high doses of the agent are administered to increase the contrast, which can induce toxicity to tissue and organs.<sup>15</sup>

To circumvent these issues, contrast agents exploiting other nuclei have been developed and tested as direct labels in MR imaging. Among those,  $^{19}\text{F}$ -based MRI has attracted much attention due to a few unique characteristics.  $^{19}\text{F}$  nuclei exhibit high gyromagnetic ratio (comparable to that of protons), yielding pronounced NMR signal, and it has 100% natural abundance. Furthermore, due to the very low traces of intrinsic fluorine in biological tissues and organs, fluorine-rich tracers can be easily visualized *in vivo* using  $^{19}\text{F}$ -based MRI, and

Received: March 7, 2022

Revised: March 30, 2022

Published: April 21, 2022



provide bright signal compared to their surroundings (i.e., positive CAs).<sup>1,3,18</sup> Indeed, it has been reported that because C–F bonds involve  $\pi$ – $\pi_F$  interactions they exhibit high enthalpy, which imparts onto them a stabilizing energy up to  $\sim 25$  kJ/mol.<sup>17</sup> This makes fluorine-rich molecules chemically and thermally more stable in biological media compared to their hydrocarbon counterparts; this has in fact led to the development of novel plastics, surfactants, and pharmaceuticals.<sup>18</sup> Early work by Holland and co-workers in 1977 suggested the feasibility of  $^{19}\text{F}$  imaging using sodium fluoride and perfluorotributylamine.<sup>19</sup> Subsequently,  $^{19}\text{F}$ -based MR has been actively investigated.<sup>1–3,16</sup> The low trace amount of intrinsic signal in biological systems presents a unique advantage which has been exploited, for example, to realize quantitative cell trafficking and physiology assessments.<sup>1,20</sup> In addition,  $^{19}\text{F}$  NMR signatures cover a wide range of chemical shifts which can be sensitive to pH changes and oxygen concentration (i.e., oxygen tension,  $p\text{O}_2$ ).<sup>21,22</sup> Transition-metal complexes containing  $^{19}\text{F}$  have also been developed as MR pH sensors.<sup>23</sup>

Perfluorocarbons (PFCs) have been widely investigated for designing  $^{19}\text{F}$  CAs. For example, hexafluorobenzene (HFB) was used to map the oxygen tension in rabbit breast tumors.<sup>24</sup> Perfluorooctyl bromide (PFOB) and its derivatives were reported to be inert and safe for use in visualizing the gastrointestinal tract.<sup>25</sup> Perfluorinated crown ether (PFCE) and perfluoropolyether (PFPE) emulsions are currently state-of-art candidates for use in biological and preclinical studies.<sup>3,16</sup> However, one of the drawbacks of these PFC-based tracers is their very limited solubility in water. They tend to aggregate in biological environments, resulting in long retention times with associated toxicity.<sup>26</sup> To address these problems, spatially structured CAs have been designed, including micelle structures formed using amphiphilic molecules that present fluorine-rich hydrophobic tails or poly(acrylic acid) containing fluorinated acrylate (or methacrylate) moieties.<sup>27</sup> Dendritic polyamidoamine (PAMAM) macromolecules prepared with large numbers of  $^{19}\text{F}$  atoms have been tested for encapsulating drugs, while allowing controlled release.<sup>28</sup> In addition, a range of partially fluorinated polymers (PFPPs) have been explored as  $^{19}\text{F}$ -based CAs.<sup>29–32</sup> Nonetheless, the high fluorine content (up to  $\sim 30$  wt %) in these tracers has often resulted in serious solubility issues in biological conditions, implying that developing  $^{19}\text{F}$  CAs with high signal-to-noise ratio and better affinity to water is still as needed as ever.

In this report, we detail the synthesis, optimization, and characterization of fluorine-rich polymers and further test their ability to provide a promising new  $^{19}\text{F}$  CA with a single NMR signature. Our design yields a set of polymer compounds that exhibit large signal-to-noise ratios, tunable  $T_2$  (and  $T_1$ ) relaxation times, all without severely compromising affinity to water solutions. Construction of these compounds exploits and builds on previous work designing multifunctional polymers, as high affinity metal-coordinating ligands to stabilize an array of inorganic nanocrystals in various solution phases, including aqueous as well as organic media.<sup>33–39</sup> It exploits the effectiveness of the nucleophilic addition reaction between amine-R nucleophiles and anhydride monomers along a poly(isobutylene-*alt*-maleic anhydride), PIMA, copolymer to introduce a combination of fluorine-rich moieties and hydrophilic (polyethylene glycol, PEG) blocks in a single macromolecule. The design allows the introduction of a high

concentration of  $^{19}\text{F}$  atoms per chain while promoting high affinity to water. Furthermore, through discrete manipulation of the macromolecular architecture, we are able to introduce additional dynamic segmental mobility of the fluorinated moieties. This results in a sizable increase in the relaxation time coupled with narrowing of the generated  $^{19}\text{F}$  NMR peak, along with a substantial enhancement in the measured intensity. The anticipated structures of the targeted compounds are confirmed using  $^1\text{H}$  NMR measurements, which provide accurate estimates of the PEG and fluorine moieties in a given polymer stoichiometry.

## RESULTS AND DISCUSSION

**Rationale.** One of the most important constraints affecting the development of  $^{19}\text{F}$ -based CAs for use in MRI and its application in biology and medicine has been the rather limited solubility in hydrophilic media. Earlier approaches explored, among others, the use of perfluorocarbon compounds as  $^{19}\text{F}$  CAs.<sup>40</sup> However, reports of heavy accumulation of intravenous administered PFCs in organs such as liver and spleen, combined with very slow biological clearance, have raised serious safety concerns about the use of these agents.<sup>41</sup> Furthermore, the lack (or absence) of chemically equivalent fluorine atoms in PFCs has yielded multiple discrete  $^{19}\text{F}$  MR signatures in a single spectrum.<sup>42</sup> This has complicated the buildup of MR images that are free of chemical shift artifacts.<sup>41,42</sup> More recently, several informative studies, reported over the past decade by Whittaker and co-workers, have introduced several polymer-based  $^{19}\text{F}$  MR CAs, including branched fluorinated glycopolymers, amphiphilic polymers capable of forming core–shell nanoparticles, and perfluoropolyether (PFPE)-based hyperbranched polymer nanoparticles.<sup>26,43–45</sup> These materials are designed using either fluorinated hydrophilic monomer precursors during the polymer synthesis or attaching hydrophilic blocks to fluorine-rich moieties.<sup>26,43–45</sup> The group has further explored the modification of the CA by, for example, introducing aptamers targeting cancer cells and tissue, to impart biological targeting capacity to the polymer CAs. However, independent of the exact chemical approach used, most  $^{19}\text{F}$ -based CAs still tend to aggregate in aqueous media even at small to moderate concentrations, which reduces the NMR signal-to-noise ratios, while drastically shortening *in vivo* blood circulation time.<sup>46</sup> This problem is directly attributed to the chemical nature of fluorinated compounds, either pure or embedded into more complex molecular structures.

**Fluorinated Polymer Design.** Our approach for addressing these issues relies on the addition reaction, to simultaneously introduce fluorinated moieties and hydrophilic PEG blocks onto a low molecular weight polymaleic anhydride copolymer, with a random arrangement of the fluorinated moieties and hydrophilic PEG blocks along the chain. More precisely, we have used two sets of fluorinated amine-R nucleophiles. The first is the commercially available 3,3,3-trifluoropropylamine (TFPA). The second is synthesized in our laboratory by inserting a tunable size, bis-reactive polyethylene glycol segment (i.e., a PEG linker/arm) between the primary amine and the  $\text{CF}_3$  label. We then rely on the addition reaction to install combinations of either  $\text{CF}_3$  and PEG-OMe moieties or PEG- $\text{CF}_3$  and PEG-OMe blocks laterally along the polymer backbone. We note that inserting a PEG-arm in the second set of fluorinated polymers should also enhance affinity to water. This strategy achieves controlled

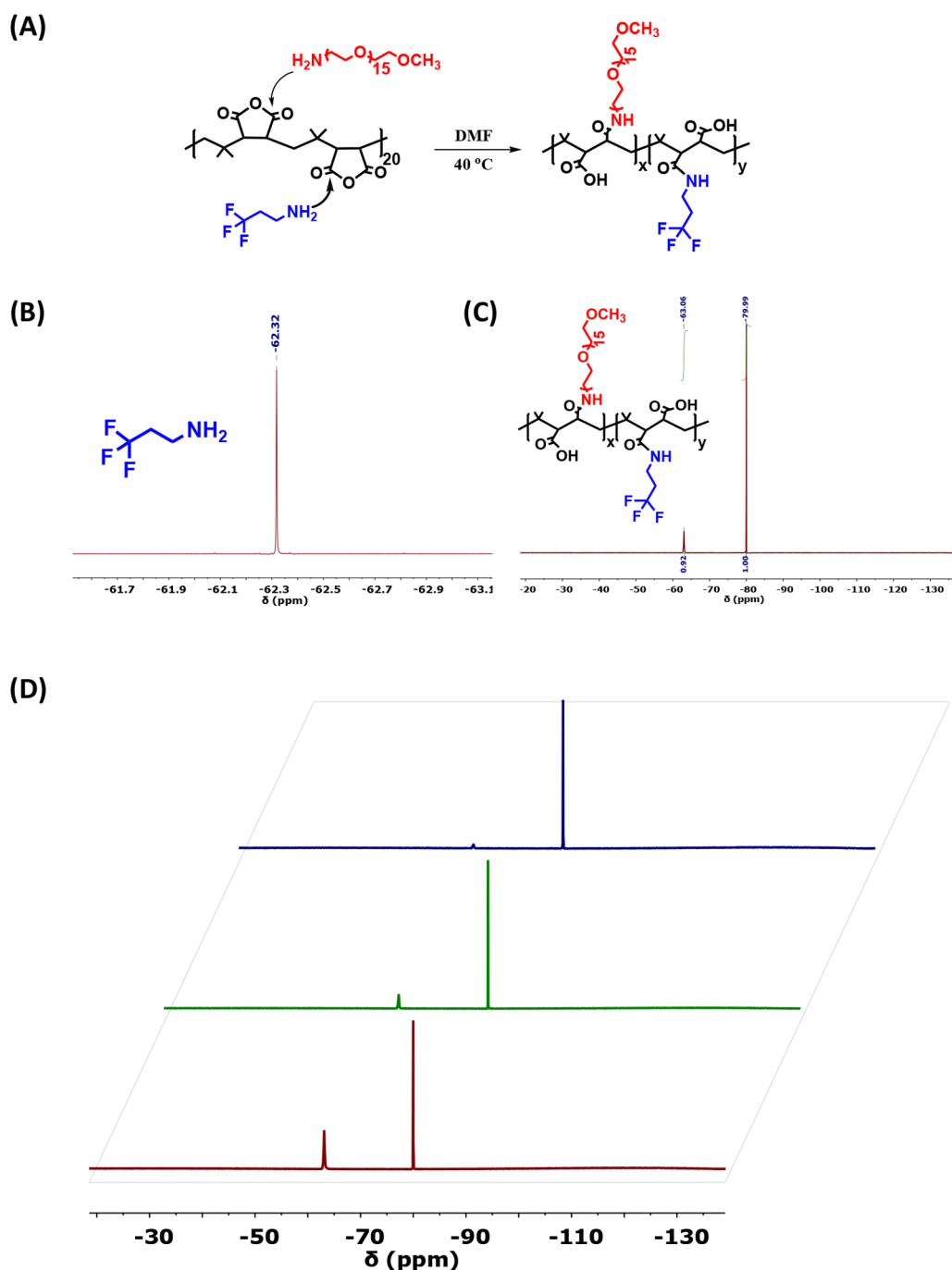


**Figure 1.** (A) Schematic representation of the nucleophilic addition reaction used to prepare the multifunctional polymer ligand PEG-OMe-PIMA-CF<sub>3</sub>. (B) <sup>19</sup>F NMR spectrum of 3,3,3-Trifluoropropylamine collected in DMSO-*d*<sub>6</sub>. (C) <sup>19</sup>F NMR spectrum of PEG-OMe-PIMA-CF<sub>3</sub>(30%) collected in DMSO-*d*<sub>6</sub>. The two peaks at ~ -63 and ~ -80 ppm designate CF<sub>3</sub> groups on the polymer and hexafluoroacetone standard, respectively. (d) Stacked <sup>1</sup>H NMR spectra of PEG-OMe-PIMA-CF<sub>3</sub>(10%, blue), PEG-OMe-PIMA-CF<sub>3</sub>(30%, green), and PEG-OMe-PIMA-CF<sub>3</sub>(50%, red) in the presence of HFA standard measured in DMSO-*d*<sub>6</sub>.




stoichiometry and random arrangement of the CF<sub>3</sub> groups along the polymer chain. We extract estimates of T<sub>2</sub> relaxation for polymers with different PEG arm-lengths between the backbone and the fluorine moieties, which confirm that the PEGylated linkers provide substantially increased <sup>19</sup>F resonance signal while narrowing the full width at half-maximum (fwhm) peak profiles.

Figure 1A shows a schematic representation of the nucleophilic addition reaction used to prepare the first set of

fluorinated polymers, PEG-OMe-PIMA-CF<sub>3</sub>. Synthesis of the CA is realized by reacting PIMA with a mixture of commercially available TFPA and an amine-modified PEG chain (amine-PEG<sub>750</sub>-OMe), prepared following the steps reported in previous protocols.<sup>47</sup> We have shown that this synthetic approach allows tuning of the polymer stoichiometry by adjusting the molar ratio(s) of the precursors with respect to the number of monomers in a PIMA chain.<sup>36</sup> Here, the <sup>1</sup>H NMR spectra acquired using solutions in DMSO show well-

defined signatures at 3.24 and 0.95 ppm ascribed to the terminal methoxy protons of PEG<sub>750</sub>-OMe blocks and methyl protons of the PIMA backbone, respectively (see Supporting Information, Figures S2 and S3). Those spectra also show a broad peak at 2.41 ppm ascribed to the methylene adjacent to the CF<sub>3</sub> groups. Integration of the signatures at 2.41 ppm for TFGA and at 3.24 ppm for PEG-OMe are compared side-by-side to that measured for the PIMA methyl groups (at ~0.95 ppm), yielding an estimate for the polymer stoichiometry. In particular, a PEG-OMe:CF<sub>3</sub> molar ratio  $x:y \sim 70:30$  is measured for PEG-OMe(70%)-PIMA-CF<sub>3</sub>(30%), while  $x:y \sim 50:50$  is deduced for PEG-OMe(50%)-PIMA-CF<sub>3</sub>(50%). More precisely, the solution <sup>1</sup>H NMR data yields ~12 CF<sub>3</sub> and ~27 PEG-OMe for the compound PEG-OMe(70%)-PIMA-CF<sub>3</sub>(30%). Similarly, we estimate ~20 CF<sub>3</sub> and ~20 PEG-OMe groups per chain for PEG-OMe(50%)-PIMA-CF<sub>3</sub>(50%) compound. These values are in good agreement with those expected from the starting molar amounts and assuming a near-complete reaction.<sup>35</sup> <sup>19</sup>F NMR spectra collected from solutions of the fluorine precursor and the final polymer are shown in Figure 1B and C. Hexafluoroacetone trihydrate (HFA, which has a signature at ~ -80 ppm) was added to the solution, as an internal standard, at a fluorine concentration comparable to that anticipated for the CA (see Experimental Section for additional details). The clearly defined peak at ~ -62 ppm is preserved in the product, albeit with a slight upfield shift to ~ -63 ppm, which indicates that the fluorine labels have been successfully installed in the polymer structure. Additionally, the approximate one-to-one ratio between the integrals of the peaks measured for the polymer and HFA is consistent with the nominal fluorine concentration expected for the stoichiometry of the prepared polymer and the standard (see Figure 1C). These results prove that the addition reaction strategy can successfully install fluorine labels and PEG-OMe blocks along the PIMA chain, with controllable stoichiometry. Nonetheless, inspection of the data shown in Figure 1C indicate a rather small fluorine signal is measured for this polymer compared to the internal standard. We next test the effect of increasing the molar percentage of fluorine groups in the polymer on the measured signal. For this we have prepared three polymer compounds with three different molar fractions of CF<sub>3</sub>, namely, 10%, 30%, and 50% (i.e., ~4, 12, and 20 CF<sub>3</sub> per macromolecule). Then, aliquots of the polymer solutions in DMSO-*d*<sub>6</sub> (20 mg/mL) have been used to collect the NMR spectra (shown in Figure 1, panel D). Table 1 summarizes the intensity ratios extracted from the NMR data for the three sets of solutions compared to the one extracted for the HFA standard. The measured intensity increases with higher fluorine content, as expected (0.03, 0.09, and 0.27 for CF<sub>3</sub> molar fractions of 10%, 30% and 50%, respectively). However, the overall NMR intensity stays rather small for these sets of polymers. Additionally, white light images acquired from solutions containing 50 mg/mL of the polymer compounds in aqueous solutions shows signs of aggregation for the polymers with higher fluorine content (PEG-OMe(50%)-PIMA-CF<sub>3</sub>(50%); see Table 1). This can be attributed to a reduced affinity of polymers with higher fluorine content to water media. We attribute the rather small NMR signal for these compounds to the slow dynamic segmental mobility of the CF<sub>3</sub> groups, due to their close proximity to the polymer backbone, a result similar to the weak peak measured for the methyl protons along the PIMA-chain (e.g., see Figures S2 and S3).<sup>39</sup>

**Table 1.** <sup>19</sup>F NMR Signal-to-Noise Ratio (SNR) Extracted from Solutions of Polymers (with a Concentration = 50 mg/mL) Prepared at the Indicated Molar Fraction of CF<sub>3</sub> Groups with Respect to the PIMA Monomers<sup>a</sup>

Polymer	SNR <sup>a</sup>	Image (50 mg/mL)
PEG-OMe-PIMA-CF <sub>3</sub> (10%)	0.03	
PEG-OMe-PIMA-CF <sub>3</sub> (30%)	0.09	
PEG-OMe-PIMA-CF <sub>3</sub> (50%)	0.27	

<sup>a</sup>Data show an increase in SNR that is commensurate with the molar fraction of CF<sub>3</sub>. The provided values are calculated with respect to the signal of the internal standard. The white-light images are acquired from PEG-OMe-PIMA-CF<sub>3</sub> solutions.

### Optimizing the Architecture of the Polymer Contrast Agent.

We next seek to increase the signal-to-noise ratio measured for the polymer CA, by introducing a PEG linker between the backbone and the fluorine groups. We reasoned that using a PEG block as linker (instead of an alkyl one) would ultimately enhance the dynamic segmental mobility of the terminal CF<sub>3</sub>, thus increasing the <sup>19</sup>F peak intensity while potentially improving the polymer affinity to water. This rationale is supported by the large difference in the proton signatures emanating from the methyl groups in the terminal methoxy of the PEG-OMe blocks (at ~3.24 ppm) compared to the one measured for the methyl groups along the backbone (at ~0.95 ppm), as shown in Figure S2 and Figure S3. The peak at 3.24 ppm is larger than the one at 0.95 ppm, even though there are fewer OMe-associated protons compared to the number of PIMA methyl protons.<sup>39</sup>

We now test the effects of inserting a varying size PEG linker between the CF<sub>3</sub> group and the primary amine to generate a new amine-PEG-CF<sub>3</sub> nucleophile, instead of relying on a commercially available NH<sub>2</sub>-alkyl-CF<sub>3</sub> compound. For a typical amine-PEG-CF<sub>3</sub>, namely, NH<sub>2</sub>-PEG<sub>600</sub>-CF<sub>3</sub>, a starting bis-reactive NH<sub>2</sub>-PEG<sub>600</sub>-N<sub>3</sub> is converted into COOH-PEG<sub>600</sub>-N<sub>3</sub> using succinic anhydride; the NH<sub>2</sub>-PEG<sub>600</sub>-N<sub>3</sub> is prepared following the steps detailed in our previous protocols.<sup>48,49</sup> The terminal carboxylic acid is coupled to TFGA in the presence of 1,1'-carbonyldiimidazole (CDI), and then the azide in the resulting CF<sub>3</sub>-PEG<sub>600</sub>-N<sub>3</sub> is reduced to NH<sub>2</sub> using Staudinger reduction, ultimately yielding a new NH<sub>2</sub>-PEG<sub>600</sub>-CF<sub>3</sub> nucleophile. Details about the synthesis are outlined in the Supporting Information; see Schematic 1. Figure 2A schematically summarizes the nucleophilic addition reaction between PIMA and a mixture of NH<sub>2</sub>-PEG<sub>750</sub>-OMe and NH<sub>2</sub>-PEG<sub>600</sub>-CF<sub>3</sub>. The <sup>19</sup>F NMR spectra shown in Figure 2, panels B,C, confirm the successful insertion of the PEGylated fluorine moieties in the NH<sub>2</sub>-PEG-CF<sub>3</sub> precursor and in the new PEG-OMe-PIMA-PEG<sub>600</sub>-CF<sub>3</sub> polymer, with a clear well-defined peak at ~ -62 ppm for both. Furthermore, comparing the <sup>19</sup>F peak intensities measured for NH<sub>2</sub>-PEG<sub>600</sub>-CF<sub>3</sub> and PEG-OMe-PIMA-PEG<sub>600</sub>-CF<sub>3</sub> to those shown in Figure 1C (no arm) clearly indicates a pronounced boosting in the NMR signal by nearly 1 order of magnitude, as a result of the change in the polymer structure, compared to the case without a PEG linker shown in Figure 1. This sizable improvement is attributed to the increased segmental mobility of the terminal

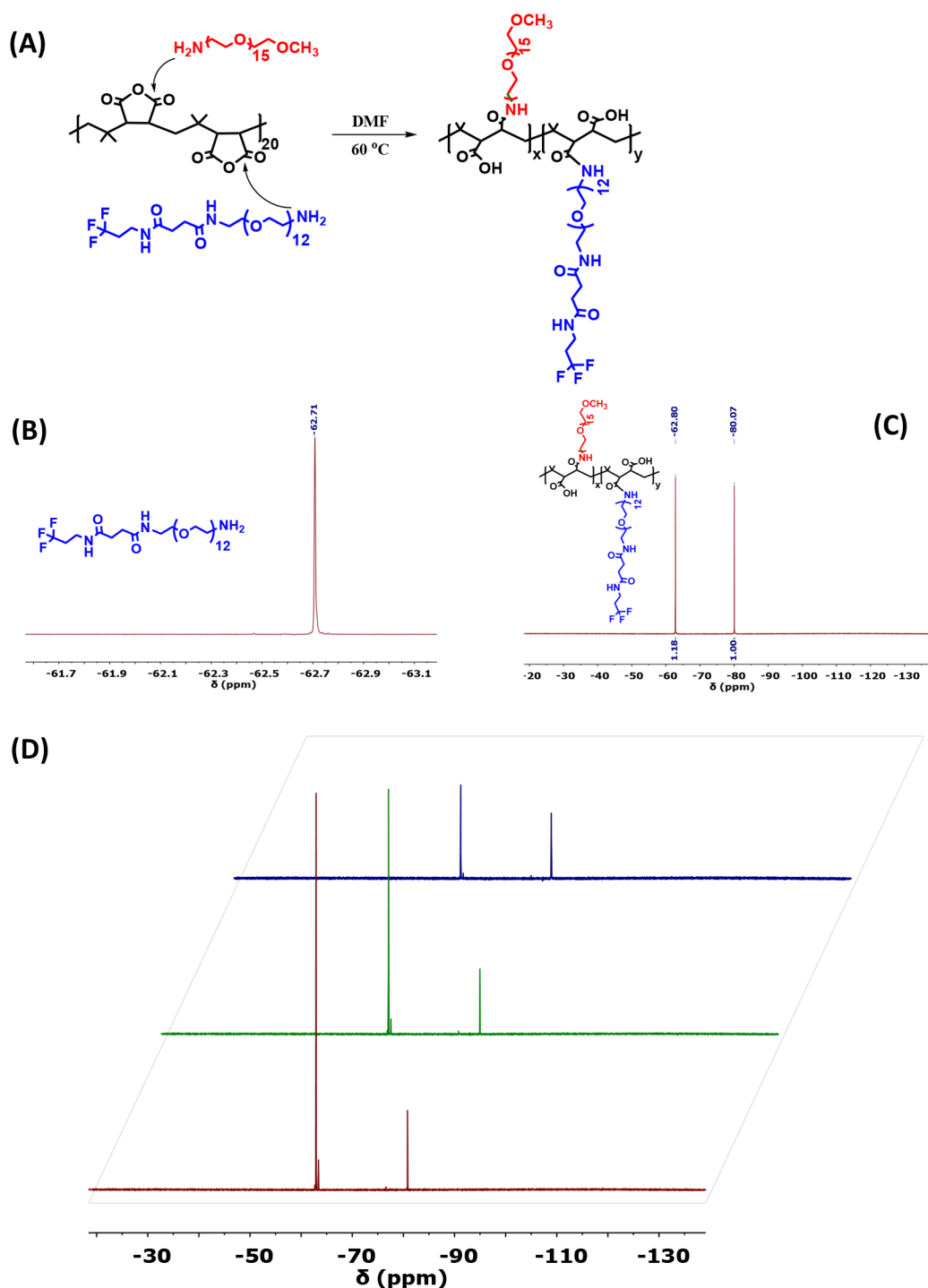





**Figure 2.** (A) Schematic representation of the addition reaction used to prepare PEG-OMe-PIMA-PEG<sub>600</sub>-CF<sub>3</sub>. (B) <sup>19</sup>F NMR spectrum of NH<sub>2</sub>-PEG<sub>600</sub>-CF<sub>3</sub> collected in DMSO-*d*<sub>6</sub>. (C) <sup>19</sup>F NMR spectrum of PEG-OMe-PIMA-PEG<sub>600</sub>-CF<sub>3</sub> collected in DMSO-*d*<sub>6</sub>. The spectrum in panel C shows two peaks at ~ -62.8 ppm and ~ -80 ppm which are ascribed to the CF<sub>3</sub> groups in the polymer and hexafluoroacetone standard, respectively. (D) Stacked <sup>19</sup>F NMR spectra of PEG-OMe-PIMA-PEG<sub>600</sub>-CF<sub>3</sub> (10%, blue), PEG-OMe-PIMA-PEG<sub>600</sub>-CF<sub>3</sub> (30%, green), PEG-OMe-PIMA-PEG<sub>600</sub>-CF<sub>3</sub> (50%, red), measured in DMSO-*d*<sub>6</sub> in the presence of HFA.

CF<sub>3</sub> groups in the new polymer. Similar to what was done above for PEG-OMe-PIMA-CF<sub>3</sub>, we have investigated the effects of the fluorine content in the polymer on the measured intensity of the NMR signal. The data shown in Figure 2D indicate that all three sets of polymers yield substantially higher signals compared to those acquired from polymers without the PEGylated linker. We have also visually inspected the clarity of

solutions of these compounds in water. We find that despite the increase in the signal-to-noise ratio, the polymer solutions with the highest fluorine content PEG-OMe(50%)-PIMA-PEG<sub>600</sub>-CF<sub>3</sub>(50%) still show a slightly cloudy appearance under white light exposure. It implies that although the PEG linker improves affinity to water, potential small aggregates may still form at high concentrations (see Table 2). We have

**Table 2.**  $^{19}\text{F}$  NMR Signal-to-Noise Ratio Acquired for PEG-OMe-PIMA-PEG<sub>600</sub>-CF<sub>3</sub> with Varying Molar Fraction of Fluorinated Moieties (10%, 30%, and 50%)<sup>a</sup>

Polymer	SNR <sup>a</sup>	Image (50 mg/mL)
PEG-OMe-PIMA-PEG <sub>600</sub> -CF <sub>3</sub> (10%)	1.38	
PEG-OMe-PIMA-PEG <sub>600</sub> -CF <sub>3</sub> (30%)	4.10	
PEG-OMe-PIMA-PEG <sub>600</sub> -CF <sub>3</sub> (50%)	5.75	

<sup>a</sup>The white light images are acquired from the same solutions used to extract SNR values. The SNR values refer to the signal reported with respect to the internal standard.

also assessed how the presence of the PEG<sub>600</sub> arm affects the fwhm and  $T_2$  relaxation time. A side-by-side comparison of spectra measured for the polymer CAs with and without the PEG<sub>600</sub> linker is provided in Figure S4. Data clearly show that insertion of the PEG linker increases the  $T_2$  time and concomitantly reduces the peak fwhm from  $\sim 70.6$  to  $\sim 9.3$  Hz; these two parameters are related by

$$\text{FWHM} = 1/(\pi T_2) \quad (1)$$

A long relaxation time indicates higher segmental mobility, which is essential for acquiring higher MRI signals. We should note that the fwhm extracted from the data using eq 1 usually differs from the experimental value, due to the fact that heterogeneous resonances also affect the line width.<sup>50</sup>

We now evaluate the effects of adjusting the PEG linker on the measured NMR signal. For this, we focus on the polymer prepared with a fixed fluorine content (i.e., PEG-OMe(70%)–PIMA-PEG<sub>600</sub>-CF<sub>3</sub>(30%), or 12 CF<sub>3</sub> groups). In particular, we investigate how changing the PEG linker using PEG<sub>150</sub>, PEG<sub>400</sub>, PEG<sub>600</sub>, and PEG<sub>1000</sub> blocks would affect the  $T_2$  relaxation time and the fwhm of the NMR signature. NH<sub>2</sub>-PEG-CF<sub>3</sub> nucleophiles with these PEG blocks have been synthesized and purified following previous protocols;<sup>48</sup> additional details are provided in the Supporting Information. The  $^1\text{H}$  and  $^{19}\text{F}$  NMR spectra acquired from solutions of the various polymers are shown in Figures S5–S8. The transverse relaxation time  $T_2$  is measured from plots of the intensity vs echo time for solutions of the various polymers in DMSO-*d*<sub>6</sub>. The resulting intensity vs time profiles are fitted using a first-exponential decay function:

$$I_{\text{Norm}} = \exp(-t/T_2) \quad (2)$$

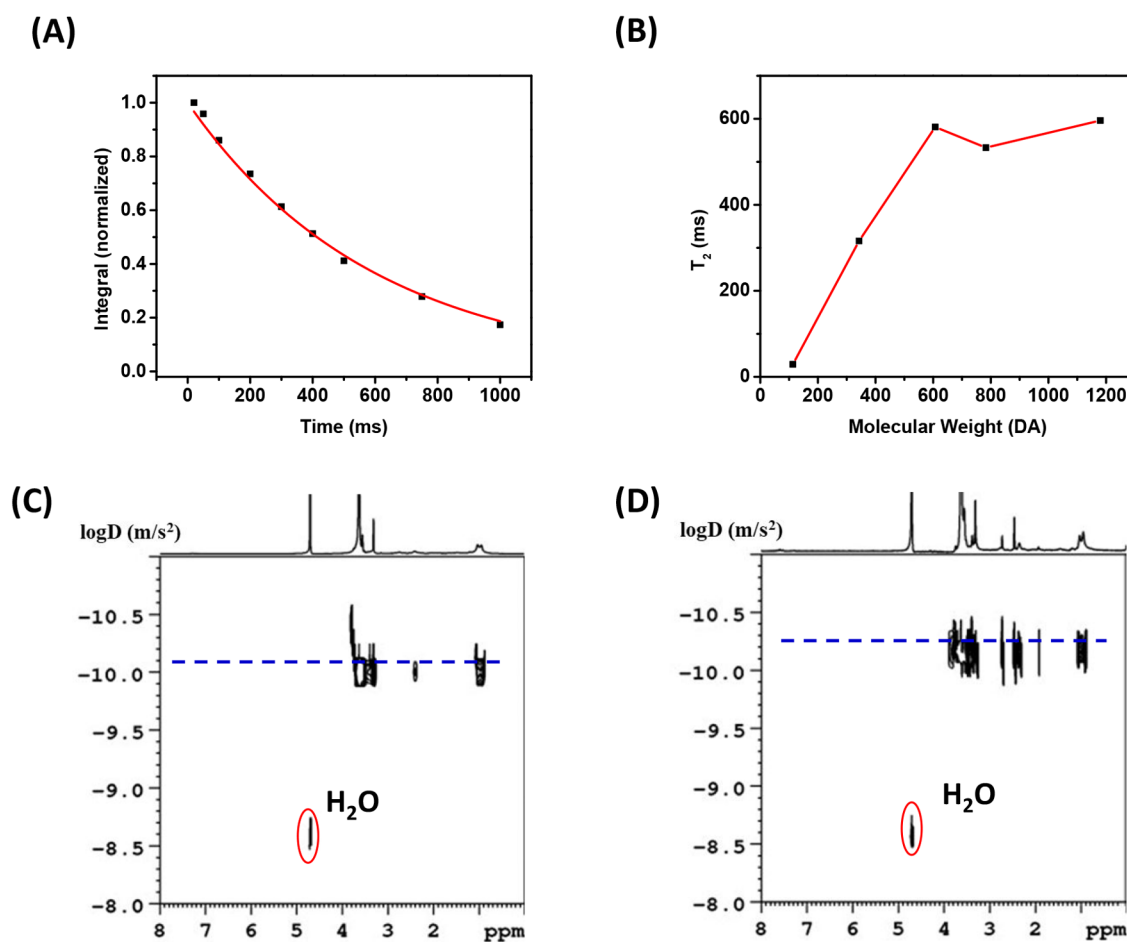


**Figure 3.** (A) Normalized integrated intensity vs echo times collected for PEG-OMe-PIMA-PEG<sub>1000</sub>-CF<sub>3</sub>. Data were fitted to an exponential decay function, yielding a decay constant ( $T_2$ ) of 596 ms. (B)  $T_2$  relaxation time vs molecular weight of the fluorinated precursors. DOSY spectra of  $\sim 10$  mg/mL PEG-OMe-PIMA-CF<sub>3</sub> (C) and PEG-OMe-PIMA-PEG<sub>600</sub>-CF<sub>3</sub> (D) are measured in D<sub>2</sub>O.

where  $I_{\text{Norm}}$  designates the normalized integrated intensity with respect to the value at  $t = 0$ , while  $T_2$  is the transverse relaxation time.  $T_2$  values ranging from 29 to 596 ms are extracted from fitting the data for the various PEG linkers, as shown in Figure 3A and Supporting Information (Figure S9). A plot of  $T_2$  vs the  $\text{NH}_2$ -PEG- $\text{CF}_3$  molecular weight shows that there is a correlation between the relaxation time and the molecular weight of the linker (see Figure 3B). Inspection of the experimental data indicates that despite the limited range of PEG linkers tested there are two trends.  $T_2$  follows a linear progression with the molecular weight from 113 to 607 Da, but saturation occurs for larger molecular weights.

**Characterizing the Polymer Hydrodynamic Dimensions.** After confirming the capacity to increase the SNR of the CAs via structural modification, we now test whether or not the use of such design would sizably increase the overall size of the polymer macromolecules. For this we performed diffusion-ordered NMR spectroscopy (DOSY-NMR) to characterize the hydrodynamic size of two representative polymer compounds: PEG-OMe-PIMA- $\text{CF}_3$  and PEG-OMe-PIMA-PEG<sub>600</sub>- $\text{CF}_3$ . DOSY-NMR is a noninvasive technique that can characterize the Brownian diffusion properties of small colloids and macromolecules.<sup>51</sup> DOSY tracks the decay (or attenuation) of the echo NMR signal intensity as a function of the magnetic field gradient,  $G_z$ , which can be described by Stejskal-Tanner relation:<sup>52,53</sup>

$$I = I(0)e^{-D\gamma^2 G_z^2 \delta^2 (\Delta - \frac{\delta}{3})} \quad (3)$$

where  $I$  designates the echo intensity measured by the detector at the end of the pulse sequence,  $\gamma$  designates the gyromagnetic ratio of the nuclei,  $G_z$  is the gradient pulse strength along the  $z$ -axis,  $\delta$  is the gradient pulse duration,  $\Delta$  is the period separating two gradient pulses, and  $D$  is the diffusion coefficient. Figure 3C,D represents the 2-D  $^1\text{H}$  DOSY contour spectra measured for the PEG-OMe-PIMA- $\text{CF}_3$  and PEG-OMe-PIMA-PEG<sub>600</sub>- $\text{CF}_3$  polymers in  $\text{D}_2\text{O}$  solutions. The corresponding intensity vs  $G_z$  profiles are provided in Figure S10. Both contour spectra show a slow diffusion coefficient ascribed to the polymer protons along with a faster diffusion coefficient emanating from the hydrogenated solvent impurities. The diffusion coefficients extracted for the two polymers are  $7.21 \times 10^{-11}$  and  $6.09 \times 10^{-11} \text{ m}^2/\text{s}$  for PEG-OMe-PIMA- $\text{CF}_3$  and PEG-OMe-PIMA-PEG<sub>600</sub>- $\text{CF}_3$ , respectively. By combining these values with the Stokes–Einstein equation:<sup>54</sup>

$$R_H = \frac{k_B T}{6\pi\eta D} \quad (4)$$

where  $k_B$  is the Boltzmann constant,  $T$  is the temperature, and  $\eta$  is the viscosity of the medium, we extract the hydrodynamic radii ( $R_H$ ) of the dissolved polymers:  $R_H \sim 3.6$  and  $4.0 \text{ nm}$  for the PEG-OMe-PIMA- $\text{CF}_3$  and PEG-OMe-PIMA-PEG<sub>600</sub>- $\text{CF}_3$ , respectively. This result suggests that inserting the PEGylated linker does not drastically affect the size of the CA.<sup>53</sup> Such small size bodes well for use in biological studies. The above set of data allow us to conclude that the polymer prepared using a fluorine precursor with a PEGylated linker of  $\sim 400$ – $600 \text{ Da}$  (i.e.,  $\text{NH}_2$ -PEG<sub>400–600</sub>- $\text{CF}_3$ ) has potentially yielded a promising CA. Inspecting aqueous solutions of PEG-OMe-PIMA-PEG<sub>600</sub>- $\text{CF}_3$  with different concentrations essentially indicates that these CAs are fully dissolved at concentrations up to  $\sim 50 \text{ mg/mL}$ , shown is Figure S11.

**Phantom MR Imaging Using the Polymer Contrast Agent.** We now proceed to assess the capacity of these  $^{19}\text{F}$ -rich polymers to provide phantom bright images in water media. Samples containing PEG-OMe-PIMA- $\text{CF}_3$  or PEG-OMe-PIMA-PEG<sub>600</sub>- $\text{CF}_3$  have been dissolved in PB buffer at varying concentrations (50, 100, 150, and 200 mg/mL) and imaged using a 900 MHz (21.1 T) MR spectrometer. First, high-resolution  $^{19}\text{F}$  gradient-recalled echo (GRE) images are acquired to clearly demonstrate that each sample in 5 mm NMR tube yields high signal intensity, as can be seen in Figure 4. Both polymer solutions exhibit increased signal intensity

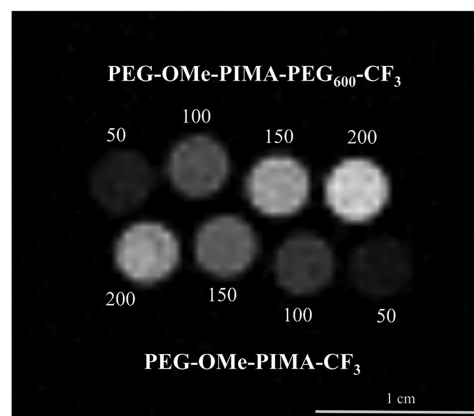


**Figure 4.** High ( $0.5 \times 0.5 \times 1.0 \text{ mm}^3$ ) resolution GRE image acquired over 4 h 19 min with  $\text{TE} = 0.846$ ,  $\text{TR} = 250 \text{ ms}$ , and 36 averages to demonstrate distinct signal intensity differences between PEG-OMe-PIMA-PEG<sub>600</sub>- $\text{CF}_3$  (top) and PEG-OMe-PIMA- $\text{CF}_3$  (bottom). Concentrations are indicated in mg/mL for each sample.

with increasing concentration. After confirming that the signal is distinguishable for all samples, the next step is to quantify the impact of introducing a PEGylated arm between the backbone and the fluorinated groups, in addition to the effect of varying the polymer concentration.

The effective  $T_2$  or  $T_2^*$  for both polymers are determined using a series of GRE images with varying echo times, TE, (1.4 to 12.0 ms) and constant recovery time, TR. The average signal intensity within a region of each sample is plotted according to echo time, and  $T_2^*$  is then extracted for each polymer and each concentration by fitting the data to a first exponential decay, as shown in Figure S12. Clearly, the introduction of the PEGylated arm greatly increases  $T_2^*$ .  $T_2^*$  also increases with increasing concentration: 6.21 vs 1.6 ms at 50 mg/mL and 27.8 vs 1.09 ms at 200 mg/mL for solutions of PEG-OMe-PIMA-PEG<sub>600</sub>- $\text{CF}_3$  and PEG-OMe-PIMA- $\text{CF}_3$  samples, respectively. Representative  $T_2$  weighted images (Figure 5) clearly show that PEG-OMe-PIMA-PEG<sub>600</sub>- $\text{CF}_3$  exhibits a higher signal intensity as compared to PEG-OMe-PIMA- $\text{CF}_3$ . The  $T_2^*$  enhancement resulting from the addition of the PEG linker implies an increased segmental mobility of  $^{19}\text{F}$  groups in the system.<sup>55</sup> We should note that measurements performed in biologically compatible buffer systems (i.e., phosphate buffer), as done here, decrease relaxation time, specifically  $T_2$ . This, and the inherent differences between  $T_2$  and  $T_2^*$ , explains the reduction in values obtained between the direct NMR measurements conducted in DMSO and MRI measurements described here. Nevertheless,  $T_2$  and  $T_2^*$  are heavily influenced by the local motion exhibited by the  $^{19}\text{F}$  nuclei, and thus increased mobility generated by the addition

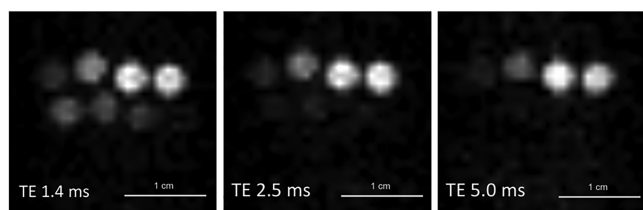


**Figure 5.** Representative images are displayed for echo times 1.4 (left panel), 2.5 ms (middle panel), and 5.0 ms (right panel). In each panel, the images in the top row are acquired from solutions of PEG-OMe-PIMA-PEG<sub>600</sub>-CF<sub>3</sub> (left to right: 50, 100, 150, 200 mg/mL), while those in the bottom are PEG-OMe-PIMA-CF<sub>3</sub> (left to right: 200, 150, 100, 50 mg/mL). Plots of the signal vs echo time for the PEG-OMe-PIMA-PEG<sub>600</sub>-CF<sub>3</sub> and PEG-OMe-PIMA-CF<sub>3</sub> are shown in the Supporting Information, Figure S12.

of a PEG linker benefits the system by increasing spin–spin relaxation.<sup>55</sup>

In addition to the impact on  $T_2^*$ , we have also assessed the effect of introducing the PEG linker on the longitudinal time,  $T_1$ , using a saturation recovery experiment.  $T_1$  values are derived from a series of GRE images with varying recovery times, 25 to 1500 ms, and constant echo time. Similar to the process described above for  $T_2^*$ ,  $T_1$  values have been extracted from the signal intensity plotted according to recovery time by fitting the data to an exponential rise to maximum, as shown in Figure S13. For equivalent concentrations,  $T_1$  remained high for the system containing the PEGylated linker as compared to the one without that linker. Comparing the evolution of  $T_1$  with polymer concentration, our data indicate that  $T_1$  decreases with increasing concentration for PEG-OMe-PIMA-PEG<sub>600</sub>-CF<sub>3</sub>, but it increases with increasing concentration for PEG-OMe-PIMA-CF<sub>3</sub>. This difference can be attributed to possible aggregation or micelle formation of the polymer in the absence of the PEG linker. Comparing both systems, the enhanced water solubility in combination with a longer  $T_2^*$  and yet a sufficiently short  $T_1$  make the PEG-OMe-PIMA-PEG<sub>600</sub>-CF<sub>3</sub> system a more suitable CA in biological applications.

To further demonstrate the imaging potential of this novel CA, <sup>19</sup>F images were acquired under short acquisition time while suspended in phosphate saline buffer to mimic biological conditions. SNR calculations using the data shown in Figure 6 to compare the effects of polymer architecture and concentration were performed on a GRE image acquired

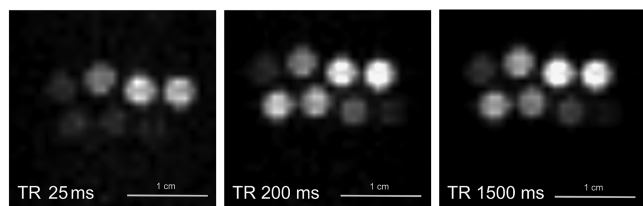


**Figure 6.** Panels show representative phantom images displayed for recovery times 25 ms (left panel), 200 ms (middle panel), and 1500 ms (right panel). In each panel, images in the top row are acquired from solutions of PEG-OMe-PIMA-PEG<sub>600</sub>-CF<sub>3</sub> (left to right: 50, 100, 150, 200 mg/mL), while the bottom ones are from solutions of PEG-OMe-PIMA-CF<sub>3</sub> (left to right: 200, 150, 100, 50 mg/mL). Plots of the signal vs echo time for the PEG-OMe-PIMA-PEG<sub>600</sub>-CF<sub>3</sub> and PEG-OMe-PIMA-CF<sub>3</sub> are shown in the Supporting Information, Figure S13.

over 5 min 45 s with TR = 25 ms and TE = 0.700 ms. A 2.5-fold increase is measured for the system with the PEG linker compared to the one without that linker at 50 mg/mL concentration; this ratio increases to a 3.45-fold at 200 mg/mL. The improved SNR for the PEG-OMe-PIMA-PEG<sub>600</sub>-CF<sub>3</sub> system confirms the results and conclusions discussed above. As result of their enhanced mobility, the fluorine moieties in PEG-OMe-PIMA-PEG<sub>600</sub>-CF<sub>3</sub> give rise to a more intense signal in MRI, compared to the polymer with short fluorinated lateral chains. The distinct difference observed in the SNR for these two CA designs strongly supports the effectiveness of introducing PEG linker chains in the chemical design, providing both enhanced water solubility and higher signal intensity.

We would like to note that the use of rather short acquisition times to collect the data shown in Figures 5 and 6 has yielded images with rather modest resolution, compared to those shown in Figure 4, for example. We would expect the SNR and resolution to be further improved with CAs based on the same strategy, but using polymers that present higher numbers of fluorinated motifs or/and moieties that present higher numbers of fluorine atoms.

## CONCLUSION

We have developed a set of water-compatible <sup>19</sup>F MRI contrast agents, by combining hydrophilic PEG blocks with fluorine-rich groups in single macromolecules, where we varied the stoichiometric ratios of those moieties as well as the architecture of the polymer. The design relies on the nucleophilic addition reaction between amine-modified PEG-OMe and PEG-CF<sub>3</sub> blocks and anhydride rings along a poly(isobutylene-*alt*-maleic anhydride) copolymer. The polymer CAs have controllable stoichiometry with good affinity to water, exhibit long  $T_2$  relaxation times, all while having compact hydrodynamic size. We have found that introducing a PEGylated linker between the backbone and the CF<sub>3</sub> groups introduces additional segmental mobility of the fluorine groups, resulting in substantial enhancement in the intensity while increasing the longitudinal relaxation,  $T_2$ . These observations suggest that the developed CAs are promising for *in vitro* and *in vivo* studies, for which biocompatibility and high MR signal are required.

We would like to note that the addition reaction applied to PIMA also offers the flexibility of introducing specific functionalities along the polymer chain (e.g., reactive sites, peptide sequences, fluorescent species), multifunctional <sup>19</sup>F CAs can be easily developed using our strategy.<sup>36,39,56</sup> Future additional modifications of CA design, based on this same polymer motif, include the use of more fluorine-rich nucleophiles. This will ultimately increase the fluorine concentration per chain and enhance the ensuing MR signals. Given the promising features exhibited by the present polymers, we envision to test their potential utility for *in vivo* imaging to visualize blood vasculature and specific organs, for example. The relatively high affinity to water is particularly attractive.

## EXPERIMENTAL SECTION

**Synthesis of PEG-OMe-PIMA-CF<sub>3</sub>.** Poly(isobutylene-*alt*-maleic anhydride) (0.5 g, 3.25 mmol monomer units) was dissolved in 3.5 mL of DMF using a 50 mL round-bottom flask equipped with a magnetic stirring bar. Then, 3,3,3-trifluoro-



propylamine (183 mg, 1.625 mmol) dissolved in DMF (500  $\mu\text{L}$ ) was added dropwise to the PIMA solution. The content was stirred for 30 min before adding  $\text{NH}_2\text{-PEG-OMe}$  (1.2 g, 1.625 mmol) dissolved in 2 mL of DMF. The reaction mixture was left stirring at 40  $^\circ\text{C}$  overnight, and then the solvent was evaporated under vacuum. The residue was redispersed in  $\text{CHCl}_3$  and purified by column chromatography also using  $\text{CHCl}_3$  as eluent, to yield the fluorinated polymer product as a yellow gel; the reaction yields was  $\sim 87\%$ .

**Synthesis of PEG-OMe-PIMA-PEG- $\text{CF}_3$ .** The protocol was applied for the synthesis of the various polymer compounds where the fluorinated groups were further separated from the PIMA chain by inserting a varying size PEG block between the backbone and the fluorine moieties, namely, PEG-OMe-PIMA- $\text{CF}_3$ , PEG-OMe-PIMA-PEG $_{150}$ - $\text{CF}_3$ , PEG-OMe-PIMA-PEG $_{400}$ - $\text{CF}_3$ , PEG-OMe-PIMA-PEG $_{600}$ - $\text{CF}_3$ , and PEG-OMe-PIMA-PEG $_{1000}$ - $\text{CF}_3$ . We describe the synthesis of PEG-OMe(50%)-PIMA-PEG $_{600}$ - $\text{CF}_3$ (50%) as a representative example. Poly(isobutylene-*alt*-maleic anhydride) (0.5 g, 3.25 mmol monomer units) was dissolved in 3.5 mL of DMF using a 50 mL round-bottom flask equipped with a magnetic stirring bar. The solution was heated to 60  $^\circ\text{C}$ , and then  $\text{NH}_2\text{-PEG}_{600}\text{-CF}_3$  (1.3 g, 1.625 mmol) dissolved in DMF (2 mL) was added to the solution. The mixture was stirred for 30 min, and then a solution of  $\text{NH}_2\text{-PEG-OMe}$  (1.2 g, 1.625 mmol) dissolved in 2 mL of DMF was added. The reaction was left stirring overnight, and the solvent was removed under vacuum. The residue was dissolved in  $\text{CHCl}_3$  and purified by column chromatography using  $\text{CHCl}_3$  as eluent, yielding the PEG-OMe-PIMA-PEG $_{600}$ - $\text{CF}_3$  as a yellow gel; the reaction yield was  $\sim 83\%$ . The above protocol provides a polymer with the stoichiometry PEG(50%)-PIMA-PEG- $\text{CF}_3$ (50%), where the percentage refers to the molar fraction of the moieties compared to the total number of monomers in the PIMA chain. To prepare the polymer compounds with other stoichiometry, the molar amounts of the precursors used during the addition reaction were adjusted accordingly.

We should note that the synthesis of the compound with the longest PEG bridge, PEG-OMe-PIMA-PEG $_{1000}$ - $\text{CF}_3$ , a small amount of DMSO ( $\sim 2$  mL) was used to increase the solubility of the reactants.

**$^{19}\text{F}$  NMR Sample Preparation.** We limit our description to the preparation of fluorinated-polymer samples used for collecting the  $^{19}\text{F}$  NMR spectra (shown in Figures 1C and 2C). Typically, to prepare a solution of PEG-OMe-PIMA- $\text{CF}_3$ ,  $\sim 6.3$  mg (0.23  $\mu\text{mol}$ ) of the polymer was dissolved in 450  $\mu\text{L}$  of DMSO- $d_6$ . To that solution, 10  $\mu\text{L}$  (1.14  $\mu\text{mol}$ ) of HFA standard stock solution was added. The latter solution was prepared by dissolving 12.5 mg of hexafluoroacetone trihydrate (HFA $\cdot 3\text{H}_2\text{O}$ ) in 500  $\mu\text{L}$  of DI water. A similar procedure was used to prepare the NMR solutions of PEG-OMe-PIMA-PEG- $\text{CF}_3$ . Typically,  $\sim 8.1$  mg (0.23  $\mu\text{mol}$ ) of the polymer was dissolved in 450  $\mu\text{L}$  of DMSO- $d_6$ , and then 10  $\mu\text{L}$  of HFA standard stock was added. We add identical amount of internal standard to both samples to confirm that the signal shown in the NMR spectra are attributed to comparable amount of fluorine content.

## ■ ASSOCIATED CONTENT

### SI Supporting Information

The Supporting Information is available free of charge at <https://pubs.acs.org/doi/10.1021/acs.bioconjchem.2c00116>.

Materials, characterization, experimental,  $^1\text{H}$  and  $^{19}\text{F}$  NMR spectra of PEG-OMe-PIMA-PEG $_{150}$ - $\text{CF}_3$ , PEG-OMe-PIMA-PEG $_{400}$ - $\text{CF}_3$ , PEG-OMe-PIMA-PEG $_{600}$ - $\text{CF}_3$ , and PEG-OMe-PIMA-PEG $_{1000}$ - $\text{CF}_3$  (PDF)

## ■ AUTHOR INFORMATION

### Corresponding Author

Hedi Mattoussi – Department of Chemistry and Biochemistry, Florida State University, Tallahassee, Florida 32306, United States; [orcid.org/0000-0002-6511-9323](https://orcid.org/0000-0002-6511-9323); Email: [mattoussi@chem.fsu.edu](mailto:mattoussi@chem.fsu.edu)

### Authors

Liang Du – Department of Chemistry and Biochemistry, Florida State University, Tallahassee, Florida 32306, United States

Shannon Helsper – The National High Magnetic Field Laboratory and FAMU-FSU Chemical and Biomedical Engineering, Florida State University, Tallahassee, Florida 32306, United States

Neda Arabzadeh Nosratabad – Department of Chemistry and Biochemistry, Florida State University, Tallahassee, Florida 32306, United States

Wentao Wang – Department of Chemistry and Biochemistry, Florida State University, Tallahassee, Florida 32306, United States; [orcid.org/0000-0003-2273-4171](https://orcid.org/0000-0003-2273-4171)

Debra Ann Fadool – Department of Biological Science, Florida State University, Tallahassee, Florida 32306, United States

Catherine Amiens – LCC-CNRS, Université de Toulouse, UPS, F-31077 Toulouse, Cedex 4, France

Samuel Grant – The National High Magnetic Field Laboratory and FAMU-FSU Chemical and Biomedical Engineering, Florida State University, Tallahassee, Florida 32306, United States; [orcid.org/0000-0001-7738-168X](https://orcid.org/0000-0001-7738-168X)

Complete contact information is available at:

<https://pubs.acs.org/doi/10.1021/acs.bioconjchem.2c00116>

### Notes

The authors declare no competing financial interest.

## ■ ACKNOWLEDGMENTS

We thank FSU, the National Science Foundation (NSF-CHE #150850 and #2005079), Air Force Office of Scientific Research (AFOSR Grant #FA9550-18-1-0144), and Asahi-Kasei Inc. for financial support. Additional support was provided by the National Institutes of Health (NIH R01-NS102395, R01-DC013080, and F31-NS115409). The content is solely the responsibility of the authors and does not necessarily represent the official views of the NIH. A portion of this work was performed at the National High Magnetic Field Laboratory, which is supported by NSF Cooperative Agreement No. DMR-1644779 and the State of Florida. We also thank Sisi Wang and Zhicheng Jin for fruitful discussions.

## ■ REFERENCES

- (1) Bulte, J. W. M. Hot spot MRI emerges from the background. *Nat. Biotechnol.* **2005**, *23*, 945–946.
- (2) Ahrens, E. T.; Flores, R.; Xu, H.; Morel, P. A. In vivo imaging platform for tracking immunotherapeutic cells. *Nat. Biotechnol.* **2005**, *23*, 983–987.
- (3) Kislukhin, A. A.; Xu, H.; Adams, S. R.; Narsinh, K. H.; Tsien, R. Y.; Ahrens, E. T. Paramagnetic fluorinated nanoemulsions for

sensitive cellular fluorine-19 magnetic resonance imaging. *Nat. Mater.* **2016**, *15*, 662–668.

(4) Na, H. B.; Song, I. C.; Hyeon, T. Inorganic Nanoparticles for MRI Contrast Agents. *Adv. Mater.* **2009**, *21*, 2133–2148.

(5) Chien, P.-H.; Feng, X.; Tang, M.; Rosenberg, J. T.; O'Neill, S.; Zheng, J.; Grant, S. C.; Hu, Y.-Y. Li Distribution Heterogeneity in Solid Electrolyte Li<sub>10</sub>GeP<sub>2</sub>S<sub>12</sub> upon Electrochemical Cycling Probed by <sup>7</sup>Li MRI. *J. Phys. Chem. Lett.* **2018**, *9*, 1990–1998.

(6) Knight, J. C.; Edwards, P. G.; Paisey, S. J. Fluorinated contrast agents for magnetic resonance imaging; a review of recent developments. *RSC Adv.* **2011**, *1*, 1415–1425.

(7) L. Villaraza, A. J.; Bumb, A.; Brechbiel, M. W. Macromolecules, Dendrimers, and Nanomaterials in Magnetic Resonance Imaging: The Interplay between Size, Function, and Pharmacokinetics. *Chem. Rev.* **2010**, *110*, 2921–2959.

(8) Debbage, P.; Jaschke, W. Molecular imaging with nanoparticles: giant roles for dwarf actors. *Histochem. Cell Biol.* **2008**, *130*, 845–875.

(9) Rosenkrantz, A. B.; Taneja, S. S. Prostate MRI Can Reduce Overdiagnosis and Overtreatment of Prostate Cancer. *Acad. Radiol.* **2015**, *22*, 1000–1006.

(10) Haffner, J.; Lemaitre, L.; Puech, P.; Haber, G.-P.; Leroy, X.; Jones, J. S.; Villers, A. Role of magnetic resonance imaging before initial biopsy: comparison of magnetic resonance imaging-targeted and systematic biopsy for significant prostate cancer detection. *BJU Int.* **2011**, *108* (8b), E171–E178.

(11) Shan, L.; Chopra, A.; Leung, K.; Eckelman, W. C.; Menkens, A. E. Characterization of nanoparticle-based contrast agents for molecular magnetic resonance imaging. *J. Nanopart. Res.* **2012**, *14*, 1122.

(12) Pan, D.; Lanza, G. M.; Wickline, S. A.; Caruthers, S. D. Nanomedicine: Perspective and promises with ligand-directed molecular imaging. *Eur. J. Radiol.* **2009**, *70*, 274–285.

(13) Wang, Y.-X. J.; Hussain, S. M.; Krestin, G. P. Superparamagnetic iron oxide contrast agents: physicochemical characteristics and applications in MR imaging. *Eur. Radiol.* **2001**, *11*, 2319–2331.

(14) Han, Z.; Cheng, H.; Parvani, J. G.; Zhou, Z.; Lu, Z.-R. Magnetic resonance molecular imaging of metastatic breast cancer by targeting extradomain-B fibronectin in the tumor microenvironment. *Magn. Reson. Med.* **2018**, *79*, 3135–3143.

(15) Tirotta, I.; Dichiarante, V.; Pigliacelli, C.; Cavallo, G.; Terraneo, G.; Bombelli, F. B.; Metrangolo, P.; Resnati, G. 19F Magnetic Resonance Imaging (MRI): From Design of Materials to Clinical Applications. *Chem. Rev.* **2015**, *115*, 1106–1129.

(16) Srinivas, M.; Turner, M. S.; Janjic, J. M.; Morel, P. A.; Laidlaw, D. H.; Ahrens, E. T. In vivo cytometry of antigen-specific T cells using 19F MRI. *Magn. Reson. Med.* **2009**, *62*, 747–753.

(17) Bacchi, S.; Benaglia, M.; Cozzi, F.; Demartin, F.; Filippini, G.; Gavezzotti, A. X-ray Diffraction and Theoretical Studies for the Quantitative Assessment of Intermolecular Arene–Perfluoroarene Stacking Interactions. *Chem.—Eur. J.* **2006**, *12*, 3538–3546.

(18) Berger, R.; Resnati, G.; Metrangolo, P.; Weber, E.; Hulliger, J. Organic fluorine compounds: a great opportunity for enhanced materials properties. *Chem. Soc. Rev.* **2011**, *40*, 3496–3508.

(19) Holland, G. N.; Bottomley, P. A.; Hinshaw, W. S. 19F magnetic resonance imaging. *J. Magn. Reson.* (1969) **1977**, *28*, 133–136.

(20) Chen, J.; Lanza, G. M.; Wickline, S. A. Quantitative magnetic resonance fluorine imaging: today and tomorrow. *Wiley Interdisciplinary Reviews: Nanomedicine and Nanobiotechnology* **2010**, *2*, 431–440.

(21) Mehta, V. D.; Kulkarni, P. V.; Mason, R. P.; Constantinescu, A.; Antich, P. P. Fluorinated Proteins as Potential 19F Magnetic Resonance Imaging and Spectroscopy Agents. *Bioconjugate Chem.* **1994**, *5*, 257–261.

(22) Nöth, U.; Rodrigues, L. M.; Robinson, S. P.; Jork, A.; Zimmermann, U.; Newell, B.; Griffiths, J. R. In vivo determination of tumor oxygenation during growth and in response to carbogen breathing using 15CS-loaded alginate capsules as fluorine-19 magnetic resonance imaging oxygen sensors. *Int. J. Radiat. Oncol. Biol. Phys.* **2004**, *60*, 909–919.

(23) Gaudette, A. I.; Thorarinsdottir, A. E.; Harris, T. D. pH-Dependent spin state population and 19F NMR chemical shift via remote ligand protonation in an iron(ii) complex. *Chem. Commun.* **2017**, *53*, 12962–12965.

(24) Xia, M.; Kodibagkar, V.; Liu, H.; Mason, R. P. Tumour oxygen dynamics measured simultaneously by near-infrared spectroscopy and 19F magnetic resonance imaging in rats. *Phys. Med. Biol.* **2006**, *51*, 45–60.

(25) Mattrey, R. F.; Trambert, M. A.; Brown, J. J.; Young, S. W.; Bruneton, J. N.; Wesbey, G. E.; Balsara, Z. N. Perflubron as an oral contrast agent for MR imaging: results of a phase III clinical trial. *Radiology* **1994**, *191*, 841–848.

(26) Zhang, C.; Moonshi, S. S.; Wang, W.; Ta, H. T.; Han, Y.; Han, F. Y.; Peng, H.; Král, P.; Rolfe, B. E.; Gooding, J. J.; et al. High F-Content Perfluoropolyether-Based Nanoparticles for Targeted Detection of Breast Cancer by 19F Magnetic Resonance and Optical Imaging. *ACS Nano* **2018**, *12*, 9162–9176.

(27) Peng, H.; Blakey, I.; Dargaville, B.; Rasoul, F.; Rose, S.; Whittaker, A. K. Synthesis and Evaluation of Partly Fluorinated Block Copolymers as MRI Imaging Agents. *Biomacromolecules* **2009**, *10*, 374–381.

(28) Criscione, J. M.; Le, B. L.; Stern, E.; Brennan, M.; Rahner, C.; Papademetris, X.; Fahmy, T. M. Self-assembly of pH-responsive fluorinated dendrimer-based particulates for drug delivery and noninvasive imaging. *Biomaterials* **2009**, *30*, 3946–3955.

(29) Wang, K.; Peng, H.; Thurecht, K. J.; Whittaker, A. K. Fluorinated POSS-Star Polymers for 19F MRI. *Macromol. Chem. Phys.* **2016**, *217*, 2262–2274.

(30) Yu, W.; Yang, Y.; Bo, S.; Li, Y.; Chen, S.; Yang, Z.; Zheng, X.; Jiang, Z.-X.; Zhou, X. Design and Synthesis of Fluorinated Dendrimers for Sensitive 19F MRI. *Journal of Organic Chemistry* **2015**, *80*, 4443–4449.

(31) Thurecht, K. J.; Blakey, I.; Peng, H.; Squires, O.; Hsu, S.; Alexander, C.; Whittaker, A. K. Functional Hyperbranched Polymers: Toward Targeted in Vivo 19F Magnetic Resonance Imaging Using Designed Macromolecules. *J. Am. Chem. Soc.* **2010**, *132*, 5336–5337.

(32) Du, W.; Nyström, A. M.; Zhang, L.; Powell, K. T.; Li, Y.; Cheng, C.; Wickline, S. A.; Wooley, K. L. Amphiphilic Hyperbranched Fluoropolymers as Nanoscopic 19F Magnetic Resonance Imaging Agent Assemblies. *Biomacromolecules* **2008**, *9*, 2826–2833.

(33) Wang, W.; Ji, X.; Du, L.; Mattoussi, H. Enhanced Colloidal Stability of Various Gold Nanostructures Using a Multicoordinating Polymer Coating. *J. Phys. Chem. C* **2017**, *121*, 22901–22913.

(34) Wang, W.; Kapur, A.; Ji, X.; Zeng, B.; Mishra, D.; Mattoussi, H. Multifunctional and High Affinity Polymer Ligand that Provides Bio-Orthogonal Coating of Quantum Dots. *Bioconjugate Chem.* **2016**, *27*, 2024–2036.

(35) Wang, W.; Kapur, A.; Ji, X.; Safi, M.; Palui, G.; Palomo, V.; Dawson, P. E.; Mattoussi, H. Photoligation of an Amphiphilic Polymer with Mixed Coordination Provides Compact and Reactive Quantum Dots. *J. Am. Chem. Soc.* **2015**, *137*, 5438–5451.

(36) Wang, W.; Ji, X.; Kapur, A.; Zhang, C.; Mattoussi, H. A Multifunctional Polymer Combining the Imidazole and Zwitterion Motifs as a Biocompatible Compact Coating for Quantum Dots. *J. Am. Chem. Soc.* **2015**, *137*, 14158–14172.

(37) Du, L.; Wang, W.; Zhang, C.; Jin, Z.; Palui, G.; Mattoussi, H. A Versatile Coordinating Ligand for Coating Semiconductor, Metal, and Metal Oxide Nanocrystals. *Chem. Mater.* **2018**, *30*, 7269–7279.

(38) Xia, C.; Wang, W.; Du, L.; Rabouw, F. T.; J. van den Heuvel, D.; Gerritsen, H. C.; Mattoussi, H.; de Mello Donega, C. Förster Resonance Energy Transfer between Colloidal CuInS<sub>2</sub>/ZnS Quantum Dots and Dark Quenchers. *J. Phys. Chem. C* **2020**, *124*, 1717–1731.

(39) Jin, Z.; Du, L.; Zhang, C.; Sugiyama, Y.; Wang, W.; Palui, G.; Wang, S.; Mattoussi, H. Modification of Poly(maleic anhydride)-Based Polymers with H<sub>2</sub>N–R Nucleophiles: Addition or Substitution Reaction? *Bioconjugate Chem.* **2019**, *30*, 871–880.

(40) Mason, R. P.; Antich, P. P.; Babcock, E. E.; Gerberich, J. L.; Nunnally, R. L. Perfluorocarbon imaging in vivo: A  $^{19}\text{F}$  MRI study in tumor-bearing mice. *Magn. Reson. Imaging* **1989**, *7*, 475–485.

(41) Stahl, T.; Mattern, D.; Brunn, H. Toxicology of perfluorinated compounds. *Environ. Sci. Eur.* **2011**, *23*, 38.

(42) Tanifum, E. A.; Patel, C.; Liaw, M. E.; Pautler, R. G.; Annappagada, A. V. Hydrophilic fluorinated molecules for spectral  $^{19}\text{F}$  MRI. *Sci. Rep.* **2018**, *8*, 2889.

(43) Zhang, C.; Moonshi, S. S.; Han, Y.; Puttick, S.; Peng, H.; Magoling, B. J. A.; Reid, J. C.; Bernardi, S.; Searles, D. J.; Král, P.; et al. PFPE-Based Polymeric  $^{19}\text{F}$  MRI Agents: A New Class of Contrast Agents with Outstanding Sensitivity. *Macromolecules* **2017**, *50*, 5953–5963.

(44) Zhang, C.; Kim, D. S.; Lawrence, J.; Hawker, C. J.; Whittaker, A. K. Elucidating the Impact of Molecular Structure on the  $^{19}\text{F}$  NMR Dynamics and MRI Performance of Fluorinated Oligomers. *ACS Macro Lett.* **2018**, *7*, 921–926.

(45) Fu, C.; Tang, J.; Pye, A.; Liu, T.; Zhang, C.; Tan, X.; Han, F.; Peng, H.; Whittaker, A. K. Fluorinated Glycopolymers as Reduction-responsive  $^{19}\text{F}$  MRI Agents for Targeted Imaging of Cancer. *Biomacromolecules* **2019**, *20*, 2043–2050.

(46) Zhang, C.; Sanchez, R. J. P.; Fu, C.; Clayden-Zabik, R.; Peng, H.; Kempe, K.; Whittaker, A. K. Importance of Thermally Induced Aggregation on  $^{19}\text{F}$  Magnetic Resonance Imaging of Perfluoropolyether-Based Comb-Shaped Poly(2-oxazoline)s. *Biomacromolecules* **2019**, *20*, 365–374.

(47) Mei, B. C.; Susumu, K.; Medintz, I. L.; Mattoussi, H. Polyethylene glycol-based bidentate ligands to enhance quantum dot and gold nanoparticle stability in biological media. *Nat. Protoc.* **2009**, *4*, 412–423.

(48) Susumu, K.; Uyeda, H. T.; Medintz, I. L.; Pons, T.; Delehanty, J. B.; Mattoussi, H. Enhancing the stability and biological functionalities of quantum dots via compact multifunctional ligands. *J. Am. Chem. Soc.* **2007**, *129*, 13987–13996.

(49) Susumu, K.; Mei, B. C.; Mattoussi, H. Multifunctional ligands based on dihydrolipoic acid and polyethylene glycol to promote biocompatibility of quantum dots. *Nat. Protocols* **2009**, *4*, 424–436.

(50) De Roo, J.; Yazdani, N.; Drijvers, E.; Lauria, A.; Maes, J.; Owen, J. S.; Van Driessche, I.; Niederberger, M.; Wood, V.; Martins, J. C.; et al. Probing Solvent–Ligand Interactions in Colloidal Nanocrystals by the NMR Line Broadening. *Chem. Mater.* **2018**, *30*, 5485–5492.

(51) Groves, P. Diffusion ordered spectroscopy (DOSY) as applied to polymers. *Polym. Chem.* **2017**, *8*, 6700–6708.

(52) Stejskal, E. O.; Tanner, J. E. Spin Diffusion Measurements: Spin Echoes in the Presence of a Time-Dependent Field Gradient. *J. Chem. Phys.* **1965**, *42*, 288–292.

(53) Zhang, C.; Jin, Z.; Zeng, B.; Wang, W.; Palui, G.; Mattoussi, H. Characterizing the Brownian Diffusion of Nanocolloids and Molecular Solutions: Diffusion-Ordered NMR Spectroscopy vs Dynamic Light Scattering. *J. Phys. Chem. B* **2020**, *124*, 4631–4650.

(54) Edward, J. T. Molecular volumes and the Stokes-Einstein equation. *J. Chem. Educ.* **1970**, *47*, 261.

(55) Munkhbat, O.; Canakci, M.; Zheng, S.; Hu, W.; Osborne, B.; Bogdanov, A. A.; Thayumanavan, S.  $^{19}\text{F}$  MRI of Polymer Nanogels Aided by Improved Segmental Mobility of Embedded Fluorine Moieties. *Biomacromolecules* **2019**, *20*, 790–800.

(56) Wang, W.; van Niekerk, E. A.; Zhang, Y.; Du, L.; Ji, X.; Wang, S.; Baker, J. D.; Groeniger, K.; Raymo, F. M.; Mattoussi, H. Compact, “Clickable” Quantum Dots Photoligated with Multifunctional Zwitterionic Polymers for Immunofluorescence and In Vivo Imaging. *Bioconjugate Chem.* **2020**, *31*, 1497–1509.

## NOTE ADDED AFTER ASAP PUBLICATION

This paper was originally published ASAP on April 21, 2022. A correction in the third paragraph of “Phantom MR Imaging Using the Polymer Contrast Agent” was made, and the paper was reposted on April 22, 2022.

## Recommended by ACS

### Fluorine Labeling of Nanoparticles and In Vivo $^{19}\text{F}$ Magnetic Resonance Imaging

Juan Manuel Arango, Mónica Carril, *et al.*

MARCH 11, 2021  
ACS APPLIED MATERIALS & INTERFACES

READ 

### Pentafluorosulfanyl ( $\text{SF}_5$ ) as a Superior $^{19}\text{F}$ Magnetic Resonance Reporter Group: Signal Detection and Biological Activity of Teriflunomide Derivatives

Christian Prinz, Sonia Waiczies, *et al.*

OCTOBER 19, 2021  
ACS SENSORS

READ 

### Exploiting the Fluxionality of Lanthanide Complexes in the Design of Paramagnetic Fluorine Probes

Randall K. Wilharm, Valérie C. Pierre, *et al.*

FEBRUARY 23, 2022  
INORGANIC CHEMISTRY

READ 

### Halogenation at the Phenylalanine Residue of Monomethyl Auristatin F Leads to a Favorable *cis/trans* Equilibrium and Retained Cytotoxicity

Iris K. Sokka, Filip S. Ekholm, *et al.*

JULY 23, 2021  
MOLECULAR PHARMACEUTICS

READ 

Get More Suggestions >